ELECTRON SPIN RESONANCE OF THE E_1' CENTER IN α-QUARTZ

By

EVANGELOS THEODORE SKOUMBOURDIS

Bachelor of Science
Tennessee Technological University
Cookeville, Tennessee
1970

Bachelor of Science
Tennessee Technological University
Cookeville, Tennessee
1972

Master of Science
Tennessee Technological University
Cookeville, Tennessee
1974

Submitted to the Faculty of the Graduate College
of the Oklahoma State University
in partial fulfillment of the requirements
for the Degree of
MASTER OF SCIENCE
December, 1982

ELECTRON SPIN RESONANCE OF THE

E_1' CENTER IN α-QUARTZ

Thesis Approved:

Larry E. Halliburton

Thesis Adviser

Marvin D. Keeter

Norman N Durham

Dean of the Graduate College

PREFACE

This study is concerned with analysis of the E.S.R. spectrum of the E_1' center defect in alpha-quartz. A model for this defect is presented.

The author wishes to express his gratitude to his major adviser, Dr. Larry E. Halliburton, for his patience and guidance throughout this study. Appreciation is also expressed to the other committee members, Dr. Geoffrey Summers, and Dr. Marvin Keener.

A note of thanks is given to Dr. Robert Bossoli for his kindness and help. Many thanks are also extended to Janet Sallee for her assistance in typing this thesis. In addition, appreciation is extended to Linda for her friendship and encouragement.

TABLE OF CONTENTS

LIST OF TABLES

LIST OF FIGURES

CHAPTER I

INTRODUCTION

Silicon dioxide (SiO_2) can take a number of different crystal structures. Among the best known are quartz, tridymite, and cristobalite (Megaw). Low quartz, commonly known as α-quartz, has the most use. Initially, we shall describe various properties of α-quartz which are needed to understand the results presented later in this thesis. A few general applications of α-quartz will also be considered in this chapter.

Piezoelectricity

The production of electrical polarization by mechanical stress is a phenomenon known as piezoelectricity (Cady, 1964). For a crystal to be piezoelectric, it must be noncentrosymmetric. This is proven by the following argument. Suppose that a centrosymmetric crystal were to be polarized by an induced stress. Consider next an inversion through the center of symmetry. The stress and the crystal exhibit no change. The induced electric polarization, however, will be reversed. We, therefore, conclude that the electric polarization is zero. Alpha-quartz is both noncentrosymmetric and piezoelectric.

Applications

Alpha-quartz is the only form of SiO_2 which has applications in precision frequency control. Also, a highly accurate method of temperature

measurement is based on the sensitivity to temperature change of the resonant frequency of an α-quartz crystal. When the crystal is cut to the proper angle, there is a linear correspondence between the resonant frequency and temperature. Sensitivities of 0.001 C^{o} are claimed for such a device. Since the measurement process relies on a frequency measurement, these devices are particularly insensitive to noise pickup in the connecting cables. Alpha-quartz is also used for surface acoustic wave (SAW) devices. Other uses include watches, computer systems, and precision bulk piezoelectric resonantors.

Crystallography

Crystallography is used to determine the geometrical structure of crystals. This enables us to tell which are noncentrosymmetric and which are centrosymmetric. The noncentrosymmetric crystals are candidates for piezoelectricity. Crystals are grouped into seven systems: They are the triclinic, monoclinic, orthorhombic, tetragonal, hexagonal, trigonal, and cubic. The one which possesses lowest symmetry is the triclinic; and the symmetry increases in ascending order with the cubic having the highest symmetry. The seven crystal systems can be categorized by thirty-two classes. Eleven out of the thirty-two are centrosymmetric and twenty are piezoelectric classes (IEEE, 1978). Eleven out of the twenty piezoelectric classes do not possess a plane of symmetry. This means that a left-handed and a right-handed form exists. Such enantiomorphous forms are mirror images of one another, neither of which can be transformed to the other by a simple rotation. Alpha-quartz is both enantiomorphous and piezoelectric.

The structure of α-quartz is made up of slightly distorted SiO_4

tetrahedra. Each corner is shared with another tetrahedron. Each silicon is surrounded by four oxygen ions and the oxygen ions are divided into two types, long and short bonds with the central silicon. The long bond is 1.612Å, the short bond is 1.606Å, and the Si-O-Si bond angle is 143.65° (Le Page et al., 1980).

Coordinate Systems

A natural coordinate system for α-quartz can be taken to consist of three axes parallel to the edges of a unit cell. Such a system does not form an orthogonal system in α-quartz. The set of axes described above is not convenient for use in calculations. Therefore, it is common practice to introduce a right-handed cartesian coordinate system for both right-handed and left-handed α-quartz. Since α-quartz has a trigonal structure, it can be characterized by a threefold symmetry axis commonly referred to as the C axis. There are also three equivalent twofold axes (a_1, a_2, a_3) that lie 120 degrees apart in a plane normal to the C axis as shown in Figure 1. This system forms a natural coordinate system for α-quartz although it contains a redundant axis. The IEEE Standard on Piezoelectricity (1978) defines the right-handed cartesian coordinate system for α-quartz by the following:

1. The Z-axis is chosen to be parallel to the C-axis. The choice of the positive direction is arbitrary.

2. One of the three equivalent a axes is chosen to represent the X axis. Practically, the positive direction of the X axis is chosen in the same direction as the positive voltage produced when the sample is released from pressure.

3. The Y axis is used to form a right-handed coordinate system for both forms of α-quartz.

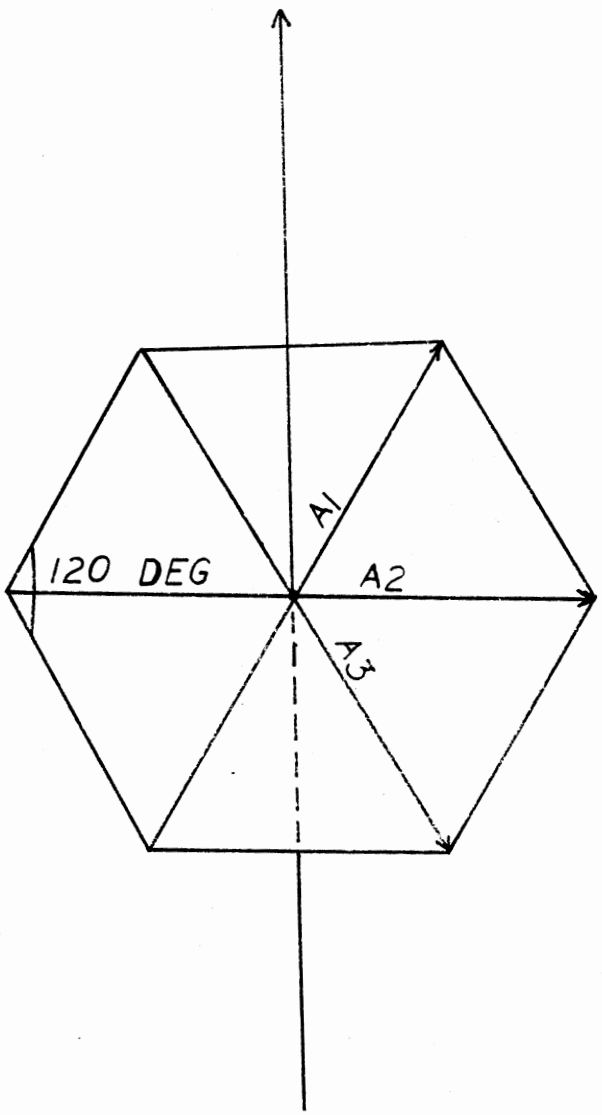

Figure 1. The Three Equivalent Twofold Axes of α-Quartz Normal to the C Axis

Oxygen Vacancy Centers in α-Quartz

Oxygen vacancies are one of the most common point defects found in α-quartz. Such vacancies are found in as-grown crystals and they can be created by neutron irradiation. It is believed that they contain two electrons (spin up and spin down, S=0) in the as-grown crystals. Ionizing radiation removes one of the electrons and leaves the oxygen vacancy with one electron (S = 1/2). These paramagnetic vacancies form a class of point defects known as E' centers.

The simplest of all the centers is referred to as the E_1' center. The general model for the E_1' center is an oxygen vacancy with one trapped electron. Weeks (1956) was the first to observe the E_1' center using the electron spin resonance (ESR) technique and Silsbee (1961) extended the study of Weeks. The theoretical work of Feigl et al. (1974) and Yip and Fowler (1975) provided us with a deeper knowledge of the electronic and ionic structure of the E_1' center. A brief discussion of some E_1' center studies is presented in the following section.

E_1' Centers

Weeks and Nelson (1960) proposed a model for the E_1' center. They proposed that an electron is trapped at an unrelaxed oxygen vacancy. Later, Silsbee (1961) presented a detailed ESR study of the E_1' centers produced by fast neutron irradiation of α-quartz. He reported the parameters for the g tensor and three hyperfine tensors. He concluded that an electron is in a nonbonding sp^3 hybrid orbital on an unrelaxed silicon. Furthermore, a pair of weak ESR hyperfine lines at about 400 gauss separation were linked to a single ^{29}Si nucleus. Feigl and Anderson reported that a single oxygen vacancy model for the E' class of centers is adequate.

Castle et al. (1963) presented a model in which an electron is trapped at a silicon located between two oxygen vacancies. Finally Yip and Fowler (1975) presented a theoretical analysis of the E_1' center in α-quartz. They used a linear combination of localized orbital-molecular orbital cluster method. Their conclusion was that an E_1' center is an electron trapped at a single oxygen vacancy. The trapped electron is strongly localized in a non-bonding sp^3 hybrid orbital centered on one silicon and is oriented along the Si-O short bond toward the oxygen vacancy. The two neighboring silicons relax asymmetrically about the oxygen vacancy; the silicon with the unpaired electron moves toward the vacancy and other silicon moves away from the vacancy (see Figure 2).

Present Study

The purpose of the present study is to characterize the ESR spectrum of the E_1' center produced by ionizing radiation in crystalline quartz. A similar study has been completed by Silsbee (1961) and our results are compared to his. Silsbee used a natural sample and created the E_1' centers by neutron irradiation. The sample in the present study is high quality synthetic quartz and the E_1' centers were produced in a very different manner.

Determination of ESR spin Hamiltonian parameters for defects in quartz have been continually plagued by misapplication of conventions for specifying principal axis directions. When relating such directions to the bond directions in the perfect lattice, it is important to follow correct and uniform definitions. Many of the past ESR studies have failed in this respect. Since the E_1' center is a primary defect in quartz and has been the subject of several theoretical studies, we believed it useful to redetermine its spin-Hamiltonian parameters.

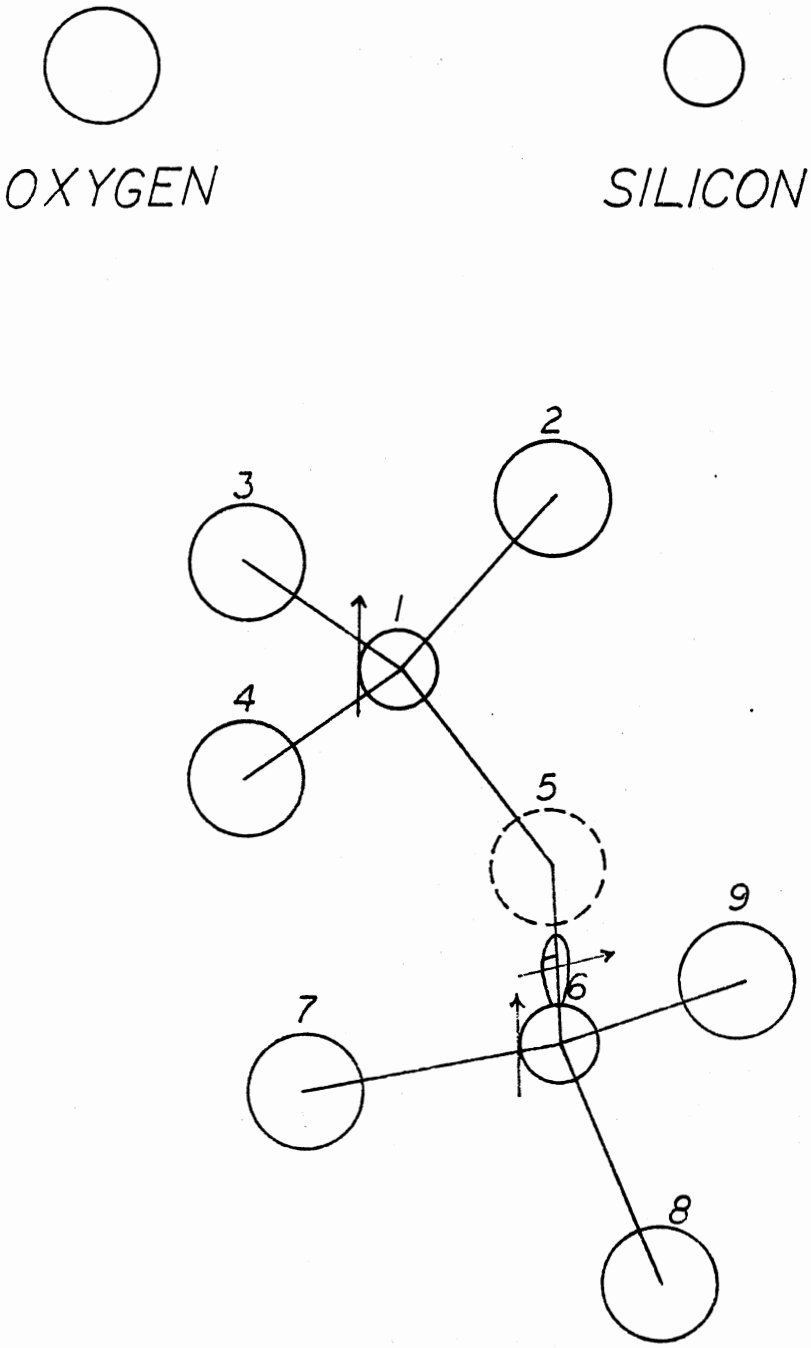

Figure 2. Yip and Fowler Model Showing Silicon Motion Toward and Away From the Vacancy

CHAPTER II

EXPERIMENTAL PROCEDURE

In this chapter the experimental procedure and equipment used to study the E_1' center is presented.

E_1' Center Production

The sample used in this study is a right-handed x-growth quartz crystal grown by Western Electric. The oxygen vacancies were introduced naturally during the growth process. To produce the E_1' centers, the sample was irradiated at room temperature for five minutes with electrons of approximately 1.7 MeV energy. Following this procedure the sample was put in an oven and heated to about $300^{\circ}C$ for a period of twenty minutes. It was then taken out of the oven and was allowed to cool to room temperature. At that stage the sample was ready to be used for the ESR study of the E_1' centers.

ESR Spectrometer

The ESR spectrometer is a device which is designed to detect unpaired electrons. Such an apparatus requires a source of microwave photon radiation and a way of detecting absorption by the sample. The spectrometer used in this experiment is a Varian X-band homodyne unit, Model V-4502. A block diagram of the ESR spectrometer's microwave bridge is shown in Figure 3.

1. KLYSTRON

2. ISOLATOR

3. MAGIC TEE

4. WAVEGUIDE

5. LOAD

6. CIRCULATOR

7. PRECISION ATTENUATOR

8. CAVITY

9. MICROWAVE SOLID STATE AMPLIFIER

10. CRYSTAL DETECTOR

11. PHASE SHIFTER

12. ATTENUATOR

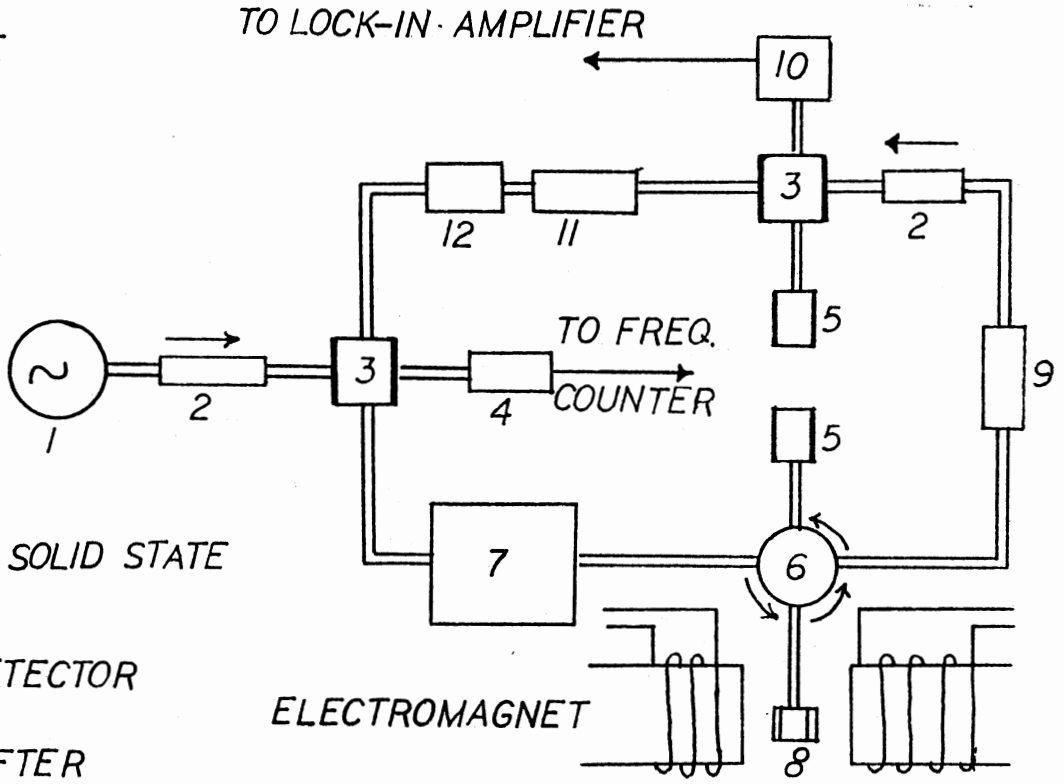

Figure 3. The ESR Spectrometer's Microwave Bridge

The microwaves are produced by a Varian VA-153C klystron. The klystron is locked to the resonant frequency of the sample cavity by the use of a reflector-modulated stabilizer. The cavity is a rectangular parallelpiped which operates in the TE_{102} mode. The microwave energy is coupled into the cavity through the iris hole. The coupling may be varied by a screw called the iris screw.

A circulator is used to direct microwave power to the cavity and to direct the reflected signal from the cavity to the detector. During operation of the spectrometer, the microwaves are kept at a fixed frequency. In the initial tuning, the klystron is adjusted over a range (i.e., a mode) since the microwave frequency is determined by the voltages applied to the klystron. A counter (HP 5340A) is used to read the microwave frequency in GHz. The isolator is a device which passes microwave energy forward, while it strongly attenuates any reflections. An attenuator is used to adjust the level of microwave power incident upon the sammple.

A Varian 9-inch V-7200 electromagnet is used to produce a static field. Field stabilization is achieved by a Hall probe mounted on one of the pole caps. The probe supplies an error signal which adjusts the magnet current to stabilize the field. The static field can be read directly from the control console; however, the readings are not precise. To remedy the situation, a proton probe is used. Since the probe cannot be mounted at the same position as the sample in the cavity, the measured static field is corrected by using a standard Cr^{3+}-doped MgO sample (known g-value equal to 1.9799). The magnetic field at the probe is read from a Varian Gaussmeter (E-500).

The magnetic field is amplitude modulated at 100 kHz by using modulation coils on each side of the cavity along the axis of the field. The

sample is mounted on a teflon mount which is attached to a precise positioning system. The teflon mount is then inserted inside the cavity allowing the sample position to be adjusted manually. Thus the static field can be put at different angles to the C-axis of the crystal. All angles are measured relative to the C axis.

CHAPTER III

THEORY

In this chapter the theoretical analysis of the ESR spectra of the E_1' center is presented. The spin Hamiltonian which describes the E_1' center is given by

$$\mathcal{H} = \beta \vec{S} \cdot \overleftrightarrow{g} \cdot \vec{H} + \vec{I} \cdot \overleftrightarrow{A} \cdot \vec{S} - g_N \beta_N \vec{H} \cdot \vec{I} \qquad (1)$$

where the first term is the electron Zeeman interaction and the second is the hyperfine interaction between an unpaired electron and the ^{29}Si magnetic nucleus (I = 1/2, 4.7% abundant). The third term represents the nuclear Zeeman interaction. We shall use the following coordinate systems to convert the Hamiltonian to a convenient form for computer programming.

x,y,z: The magnetic field coordinate system with the magnetic field parallel to the z axis.

x_1, y_1, z_1: The principal axes for the ^{29}Si hyperfine tensor.

x_g, y_g, z_g: The principal axes of the g tensor.

Rewriting the Hamiltonian using the different coordinate systems, we get

$$\mathcal{H} = \beta (S_{x_g} \; S_{y_g} \; S_{z_g}) \begin{pmatrix} g_{x_g} & 0 & 0 \\ 0 & g_{y_g} & 0 \\ 0 & 0 & g_{z_g} \end{pmatrix} \begin{pmatrix} H_{x_g} \\ H_{y_g} \\ H_{z_g} \end{pmatrix} +$$

$$(I_{x_1}, I_{y_1}, I_{z_1}) \begin{pmatrix} A_{x_1} & 0 & 0 \\ 0 & A_{y_1} & 0 \\ 0 & 0 & A_{z_1} \end{pmatrix} \begin{pmatrix} S_{x_1} \\ S_{y_1} \\ S_{z_1} \end{pmatrix} - g_N \beta_N H_z I_z . \qquad (2)$$

Note that $g_N \beta_N \vec{H} \cdot \vec{I} = g_N \beta_N H_z I_z$ since the magnetic field is parallel to the z axis. Thus;

$$\mathcal{H} = \beta[S_{n_g} g_{x_g} H_{x_g} + S_{y_g} g_{y_g} H_{y_g} + S_{z_g} g_{z_g} H_{z_g}] + [I_{x_1} A_{x_1} S_{x_1} +$$

$$I_{y_1} A_{y_1} S_{y_1} + I_{z_1} A_{z_1} S_{z_1}] - g_N \beta_N H_z I_z . \qquad (3)$$

The relationships between the coordinate systems are

$$\begin{pmatrix} x_g \\ y_g \\ z_g \end{pmatrix} = (TG) \begin{pmatrix} x \\ y \\ z \end{pmatrix} \qquad (4)$$

and

$$\begin{pmatrix} x_1 \\ y_1 \\ z_1 \end{pmatrix} = (TH) \begin{pmatrix} x \\ y \\ z \end{pmatrix} . \qquad (5)$$

The transformation matrices are as follows:

(G): Transforms the $\overleftrightarrow{g}$ tensor principal axes to the crystal coordinate system.

(H): Transforms the axes of the $\overleftrightarrow{A}$ tensor to the crystal coordinate system.

(TG): Transforms the $\overleftrightarrow{g}$ tensor principal axes to the magnetic field coordinate system.

(GH): Transforms the axes of the $\overleftrightarrow{A}$ tensor to the magnetic field coordinate system.

More explicitly, we have

$$(TG) = \begin{pmatrix} TG_{(1,1)} & TG_{(1,2)} & TG_{(1,3)} \\ TG_{(2,1)} & TG_{(2,2)} & TG_{(2,3)} \\ TG_{(3,1)} & TG_{(3,2)} & TG_{(3,3)} \end{pmatrix}, \quad (TH) = \begin{pmatrix} TH_{(1,1)} & TH_{(1,2)} & TH_{(1,3)} \\ TH_{(2,1)} & TH_{(2,2)} & TH_{(2,3)} \\ TH_{(3,1)} & TH_{(3,2)} & TH_{(3,3)} \end{pmatrix},$$

and

$$\begin{pmatrix} S_{x_g} \\ S_{y_g} \\ S_{z_g} \end{pmatrix} = \begin{pmatrix} TG_{(1,1)} & TG_{(1,2)} & TG_{(1,3)} \\ TG_{(2,1)} & TG_{(2,2)} & TG_{(2,3)} \\ TG_{(3,1)} & TG_{(3,2)} & TG_{(3,3)} \end{pmatrix} \begin{pmatrix} S_x \\ S_y \\ S_z \end{pmatrix}.$$

The spin operators then transform as follows:

$$S_{x_g} = TG_{(1,1)} S_x + TG_{(1,2)} S_y + TG_{(1,3)} S_z \tag{6}$$

$$S_{y_g} = TG_{(2,1)} S_x + TG_{(2,2)} S_y + TG_{(2,3)} S_z \tag{7}$$

$$S_{z_g} = TG_{(3,1)} S_x + TG_{(3,2)} S_y + TG_{(3,3)} S_z \tag{8}$$

The magnetic field components are given below.

$$H_{x_g} = TG_{(1,3)} H_z \tag{9}$$

$$H_{y_g} = TG_{(2,3)} H_z \tag{10}$$

$$H_{z_g} = TG_{(3,3)} H_z \tag{11}$$

We let $H = H_z$.

In terms of the x, y, z coordinate system, we can write

$$\begin{pmatrix} I_{x_1} \\ I_{y_1} \\ I_{z_1} \end{pmatrix} = \begin{pmatrix} TH_{(1,1)} & TH_{(1,2)} & TH_{(1,3)} \\ TH_{(2,1)} & TH_{(2,2)} & TH_{(2,3)} \\ TH_{(3,1)} & TH_{(3,2)} & TH_{(3,3)} \end{pmatrix} \begin{pmatrix} I_x \\ I_y \\ I_z \end{pmatrix} .$$

Thus,

$$I_{x_1} = TH_{(1,1)} I_x + TH_{(1,2)} I_y + TH_{(1,3)} I_z \tag{12}$$

$$I_{y_1} = TH_{(2,1)} I_x + TH_{(2,2)} I_y + TH_{(2,3)} I_z \tag{13}$$

$$I_{z_1} = TH_{(3,1)} I_x + TH_{(3,2)} I_y + TH_{(3,3)} I_z \tag{14}$$

and similarly,

$$S_{x_1} = TH_{(1,1)} S_x + TH_{(1,2)} S_y + TH_{(1,3)} S_z \tag{15}$$

$$S_{y_1} = TH_{(2,1)} S_x + TH_{(2,2)} S_y + TH_{(2,3)} S_z \tag{16}$$

$$S_{z_1} = TH_{(3,1)} S_x + TH_{(3,2)} S_y + TH_{(3,3)} S_z . \tag{17}$$

Now rewrite the Hamiltonian in terms of the magnetic field coordinate system as follows:

$$\mathcal{H} = \beta[\{g_{x_g} (TG_{(1,1)} S_x + TG_{(1,2)} S_y + TG_{(1,3)} S_z)(TG_{(1,3)} H)\} +$$

$$\{g_{y_g} (TG_{(2,1)} S_x + TG_{(2,2)} S_y + TG_{(2,3)} S_z) (TG_{(2,3)} H)\} +$$

$$\{g_{z_g} (TG_{(3,1)} S_x + TG_{(3,2)} S_y + TG_{(3,3)} S_z) (TG_{(3,3)} H)\}] +$$

$$A_{x_1}[\{TH_{(1,1)}I_x + TH_{(1,2)}I_y + TH_{(1,3)}I_z\}\{TH_{(1,1)}S_x + TH_{(1,2)}S_y + TH_{(1,3)}S_z\}] + A_{y_1}[\{TH_{(2,1)}I_x + TH_{(2,2)}I_y + TH_{(2,3)}I_z\}\{TH_{(2,1)}S_x + TH_{(2,2)}S_y + TH_{(2,3)}S_z\}] + A_{z_1}[\{TH_{(3,1)}I_x + TH_{(3,2)}I_y + TH_{(3,3)}I_z\}\{TH_{(3,1)}S_x + TH_{(3,2)}S_y + TH_{(3,3)}S_z\}] - g_N\beta_N HI_z . \quad (18)$$

After expanding the Hamiltonian we get

$$\begin{aligned}
\mathcal{H} = {} & \beta H[g_{x_g}\{TG(1,1)TG(1,3)S_x + TG(1,2)TG(1,3)S_y + TG(1,3)TG(1,3)S_z\} \\
& + g_{y_g}\{TG(2,1)TG(2,3)S_x + TG(2,2)TG(2,3)S_y + TG(2,3)TG(2,3)S_z\} \\
& + g_{z_g}\{TG(3,1)TG(3,3)S_x + TG(3,2)TG(3,3)S_y + TG(3,3)TG(3,3)S_z\}] \\
& + A_{x_1}[\{TH(1,1)TH(1,1)I_xS_x + TH(1,1)TH(1,2)I_xS_y + TH(1,1)TH(1,3)I_x \\
& \times S_z + TH(1,2)TH(1,1)I_yS_x + TH(1,2)TH(1,2)I_yS_y + TH(1,2)TH(1,3) \\
& \times I_yS_z + TH(1,3)TH(1,1)I_zS_x + TH(1,3)TH(1,2)I_zS_y + TH(1,3)TH(1,3) \\
& \times I_zS_z\}] + A_{y_1}[\{TH(2,1)TH(2,1)I_xS_x + TH(2,1)TH(2,2)I_xS_y + \\
& \times TH(2,1)TH(2,3)I_xS_z + TH(2,2)TH(2,1)I_yS_x + TH(2,2)TH(2,2)I_yS_y \\
& + TH(2,2)TH(2,3)I_yS_z + TH(2,3)TH(2,1)I_zS_x + TH(2,3)TH(2,2)I_zS_y \\
& + TH(2,3)TH(2,3)I_zS_z\}] + A_{z_1}[\{TH(3,1)TH(3,1)I_xS_x + TH(3,1)TH(3,2) \\
& \times I_xS_y + TH(3,1)TH(3,3)I_xS_z + TH(3,2)TH(3,1)I_yS_x + TH(3,2)TH(3,2)
\end{aligned}$$

$$x\ I_y S_y + TH(3,2)TH(3,3)I_y S_z + TH(3,3)TH(3,1)I_z S_x + TH(3,3)$$

$$x\ TH(3,2)I_z S_y + TH(3,3)TH(3,3)I_z S_z\}] - g_N \beta_N HI_z \ . \qquad (19)$$

Let the coefficient of S_x be denoted by W_1. Thus, $W_1 = \beta H[g_{x_g}$

$$TG(1,1)TH(1,3) + g_{y_g} TG(2,1)TG(2,3) + g_{z_g} TG(3,1)TG(3,3)] \ . \qquad (20)$$

Similarly, let W_2 and W_3 be thecoefficients of S_y ans S_z, respectively. Let the coefficient of $I_x S_x$ be denoted by W_4. Thus

$$W_4 = A_{x_1} TH(1,1)TH(1,1) + A_{y_1} TH(2,1)TH(2,1) + A_{z_1} TH(3,1)TH(3,1). \qquad (21)$$

Similarly, let W_5, W_6, W_7, W_8, and W_9 be the coefficients of $I_x S_y$, $I_x S_z$, $I_y S_y$, $I_y S_z$, and $I_z S_z$, respectively. Thus,

$$\mathcal{H} = W_1 S_x + W_2 S_y + W_3 S_z + W_4 I_x S_x + W_5 I_x S_y + W_6 I_x S_z$$

$$+ W_5 I_y S_x + W_7 I_y S_y + W_8 I_y S_z + W_6 I_z S_x + W_8 I_z S_y$$

$$+ W_9 I_z S_z - g_N \beta_N HI_z \ . \qquad (22)$$

Next consider the raising and lowering operators.

$$S_+ = S_x + iS_y, \qquad S_- = S_x - iS_y \qquad (23)$$

$$I_+ = I_x + iI_y, \qquad I_- = I_x - iI_y \ . \qquad (24)$$

We can write S_x, S_y, I_x, and I_y as follows:

$$S_x = \frac{(S_+ + S_-)}{2}, \quad S_y = \frac{(S_+ - S_-)}{2i}, \quad I_x = \frac{I_+ + I_-}{2}, \text{ and}$$

$$I_y = \frac{(I_+ - I_-)}{2i} . \tag{25}$$

These operators can be combined as follows:

$$I_x S_x = \frac{1}{4}(I_+ S_+ + I_+ S_- + I_- S_+ + I_- S_-) \tag{26}$$

$$I_x S_y = \frac{-i}{4}(I_+ S_+ - I_+ S_- + I_- S_+ - I_- S_-) \tag{27}$$

$$I_x S_z = \frac{1}{2}(I_+ S_z + I_- S_z) \tag{28}$$

$$I_y S_x = \frac{i}{4}(I_+ S_+ + I_+ S_- - I_- S_+ - I_- S_-) \tag{29}$$

$$I_y S_y = -\frac{1}{4}(I_+ S_+ - I_+ S_- + I_- S_+ - I_- S_-) \tag{30}$$

$$I_y S_z = -\frac{i}{2}(I_+ S_z - I_- S_z) \tag{31}$$

$$I_z S_x = \frac{1}{2}(I_z S_+ + I_z S_-) \tag{32}$$

$$I_z S_g = -\frac{i}{2}(I_z S_+ - I_z S_-) \tag{33}$$

Substituting the above expressions in the Hamiltonian and collecting terms, the Hamiltonian can be rewritten in the form

$$\mathcal{H} = W_3 S_z + W_9 I_z S_z - g_N \beta_N H I_z + Q_1^* S_+ + Q_1 S_- + Q_2^* I_+ S_+ + Q_3 I_+ S_-$$

$$+ Q_3 I_- S_+ + Q_4^* I_+ S_z + Q_4 I_- S_z + Q_4^* I_z S_+ + Q_4 I_z S_- \tag{34}$$

where

$$Q_1 = \frac{1}{2}(W_1 + iW_2) \tag{35}$$

$$Q_2 = \frac{1}{4}(W_4 - W_7) + \frac{i}{2} W_5 \tag{36}$$

$$Q_3 = \frac{1}{4}(W_4 + W_7) \tag{37}$$

$$Q_4 = \frac{1}{2}(W_6 + iW_8) \tag{38}$$

Since the ^{29}Si nucleus has $I = \frac{1}{2}$ and the unpaired electron has $S = \frac{1}{2}$, the basis set is $|M_S = \pm\frac{1}{2}, M_I = \pm\frac{1}{2}\rangle$. This basis set consists of four vectors and allows us to write the Hamiltonian in a 4x4 matrix form. Since the Hamiltonian is Hermitian, knowledge of the lower half suffices to calculate the energy eigenvalues. The lower half of the matrix is presented in Table I. The nonzero elements are determined in the following way.

$$A(1,1) = \langle +\tfrac{1}{2}, +\tfrac{1}{2} | \mathcal{H} | +\tfrac{1}{2}, +\tfrac{1}{2}\rangle = \langle +\tfrac{1}{2}, +\tfrac{1}{2} | W_3 S_z + W_9 I_z S_z - g_N \beta_N H I_z | +\tfrac{1}{2}, +\tfrac{1}{2}\rangle$$

$$= \langle +\tfrac{1}{2}, +\tfrac{1}{2} | \frac{W_3}{2} + W_9 \tfrac{1}{2}\cdot\tfrac{1}{2} - g_N \beta_N \frac{H}{2} | +\tfrac{1}{2}, +\tfrac{1}{2}\rangle$$

$$= \left[\frac{W_3}{2} + \frac{W_9}{4} - g_N \beta_N \frac{H}{2}\right] \langle +\tfrac{1}{2}, +\tfrac{1}{2} | +\tfrac{1}{2}, +\tfrac{1}{2}\rangle = \frac{W_3}{2} + \frac{W_9}{4} - \frac{g_N \beta_N H}{2} .$$

Similarly, the rest of the lower half elements of the Hermitian matrix are

$$A(2,1) = \frac{Q_4}{2} \tag{39}$$

$$A(3,1) = Q_1 + \frac{Q_4}{2} \tag{40}$$

$$A(4,1) = Q_2 \tag{41}$$

$$A(2,2) = \frac{W_3}{2} - \frac{W_9}{4} + \frac{1}{2} g_N \beta_N H \tag{42}$$

$$A(3,2) = Q_3 \tag{43}$$

$$A(4,2) = Q_1 - \frac{Q_4}{2} \tag{44}$$

$$A(3,3) = -\frac{W_3}{2} - \frac{W_9}{4} - \frac{1}{2} g_N \beta_N H \tag{45}$$

$$A(4,3) = -\frac{Q_4}{2} \tag{46}$$

$$A(4,4) = -\frac{W_3}{2} + \frac{W_9}{4} + \frac{1}{2} \beta_B g_N H \ . \tag{47}$$

TABLE I

THE LOWER HALF OF THE HAMILTONIAN MATRIX

	$\left\|+\frac{1}{2}, +\frac{1}{2}\right>$	$\left\|+\frac{1}{2}, -\frac{1}{2}\right>$	$\left\|-\frac{1}{2}, +\frac{1}{2}\right>$	$\left\|-\frac{1}{2}, -\frac{1}{2}\right>$
$\left\|+\frac{1}{2}, +\frac{1}{2}\right>$	A(1,1)			
$\left\|+\frac{1}{2}, -\frac{1}{2}\right>$	A(2,1)	A(2,2)		
$\left\|-\frac{1}{2}, +\frac{1}{2}\right>$	A(3,1)	A(3,2)	A(3,3)	
$\left\|-\frac{1}{2}, -\frac{1}{2}\right>$	A(4,1)	A(4,2)	A(4,3)	A(4,4)

CHAPTER IV

EXPERIMENTAL RESULTS

ESR Phenomena

A system with spin $S = \frac{1}{2}$ and $I = \frac{1}{2}$ is characterized by the quantum numbers $M_s = \pm\frac{1}{2}$, and $M_I = \pm\frac{1}{2}$. Such a system possesses four independent spin eigenfunctions $|M_s, M_I\rangle$. The interaction of an unpaired electron and a magnetic nucleus ^{29}Si is called a hyperfine interaction, with $\overleftrightarrow{A}$ being the hyperfine coupling matrix measured in Hz. The interaction energy between the electron and nucleus is $h\overleftrightarrow{A}$.

There are three transitions, two when the magnetic nucleus is present and one when there is no magnetic nucleus, according to the spin selection rules $\Delta M_s = \pm 1$ and $\Delta M_I = 0$. These rules can be verified by the following simple analysis. Consider the Hamiltonian

$$H = g\beta \vec{H}\cdot\vec{S} = g\beta[H_x S_x + H_y S_y + H_z S_z] . \tag{48}$$

The external magnetic field $\vec{H}$ can be written as

$$\vec{H}_{total} = \vec{H}_{static} + \vec{H}_{microwave} . \tag{49}$$

Since $\vec{H}_{static}$ is pointing in the z direction, we choose $\vec{H}_{microwave}$ to point in the x direction. Therefore, the contribution in the y direction is zero, and we have $\vec{H} = g\beta H_{microwave} (\frac{1}{2})(S_+ + S_-) + g\beta H_{static} S_z$. (50)

The transitions according to these selection rules are shown in

Figure 4. They are:

$$h\nu = D_1 - D_6 \tag{51}$$

$$h\nu = D_2 - D_5 \tag{52}$$

$$h\nu = D_3 - D_4 \tag{53}$$

The transitions (51), (52), and (53) are possible only if the electromagnetic radiation is polarized such that the oscillating magnetic field has a component perpendicular to the static field. If the oscillating magnetic field is parallel to the external field, then the effect of the radiation will be to cause an oscillation in the energies of the Zeeman levels.

Observations and Experimental Results

The principal E_1' center spectrum for the magnetic field along the [001] direction consists of one intense centered line with two pairs of weaker satellite lines centered on the central line, as shown in Figure 5. The gain of the spectrometer was reduced by a factor of 15 for the larger central line. One additional pair of satellite lines, referred to as the strong hyperfine, were observed about the central line with a splitting of 404 gauss, as shown in Figure 6. The strong hyperfine interaction is with a ^{29}Si nucleus ($I = \frac{1}{2}$, 4.7% natural abundance). As the static field is rotated away from the c-axis, each of these lines breaks up into three lines. The rotation takes place about the twofold x-axis.

A comparison of Figures 5 and 6 with Figure 4 shows that the Zeeman transition corresponds to the central line and the other two transitions

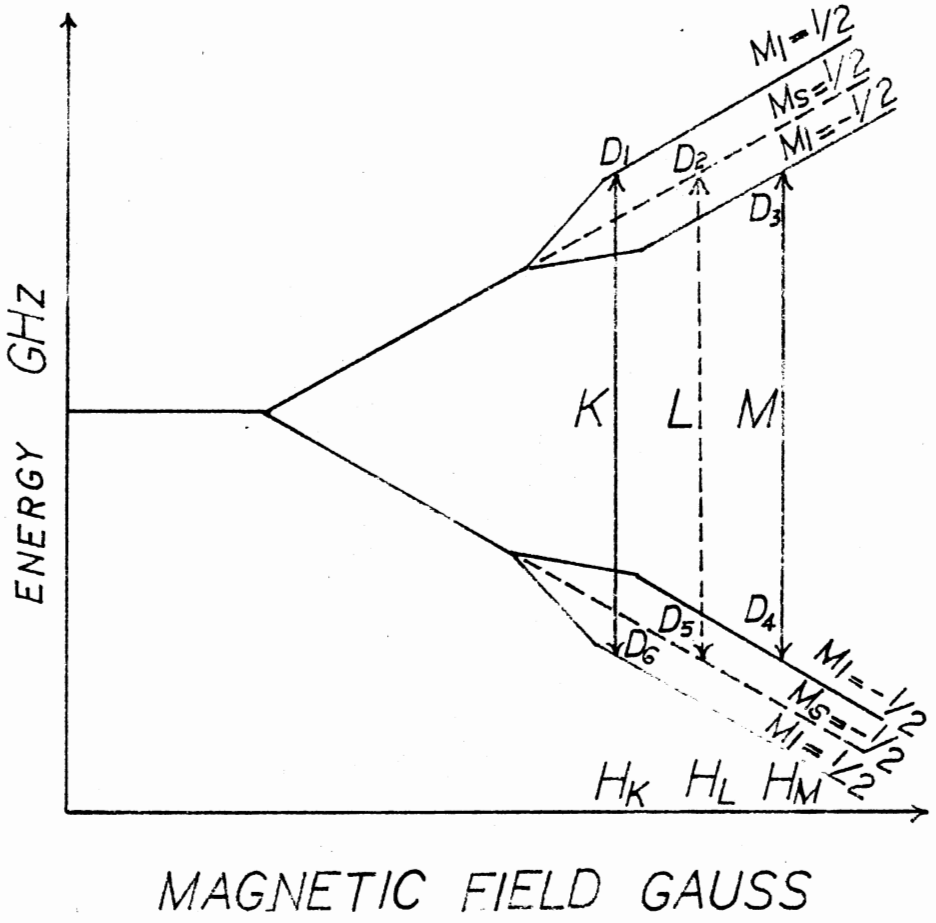

Figure 4. Energy Levels and Transitions in an S=1/2, I = 1/2 System

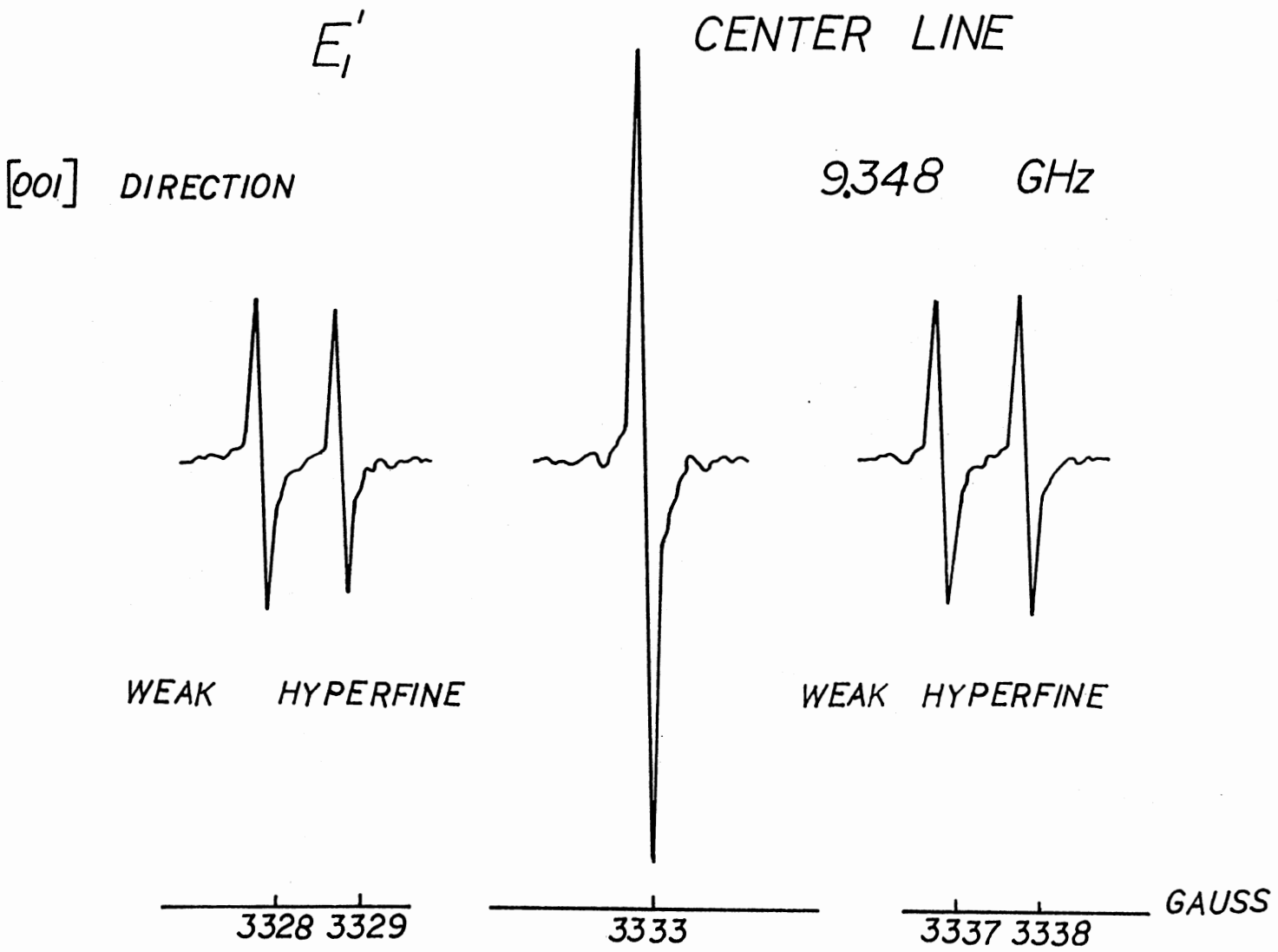

Figure 5. Principal E_1' Center Spectrum Showing the Center Line and the Weak Hyperfine Interaction

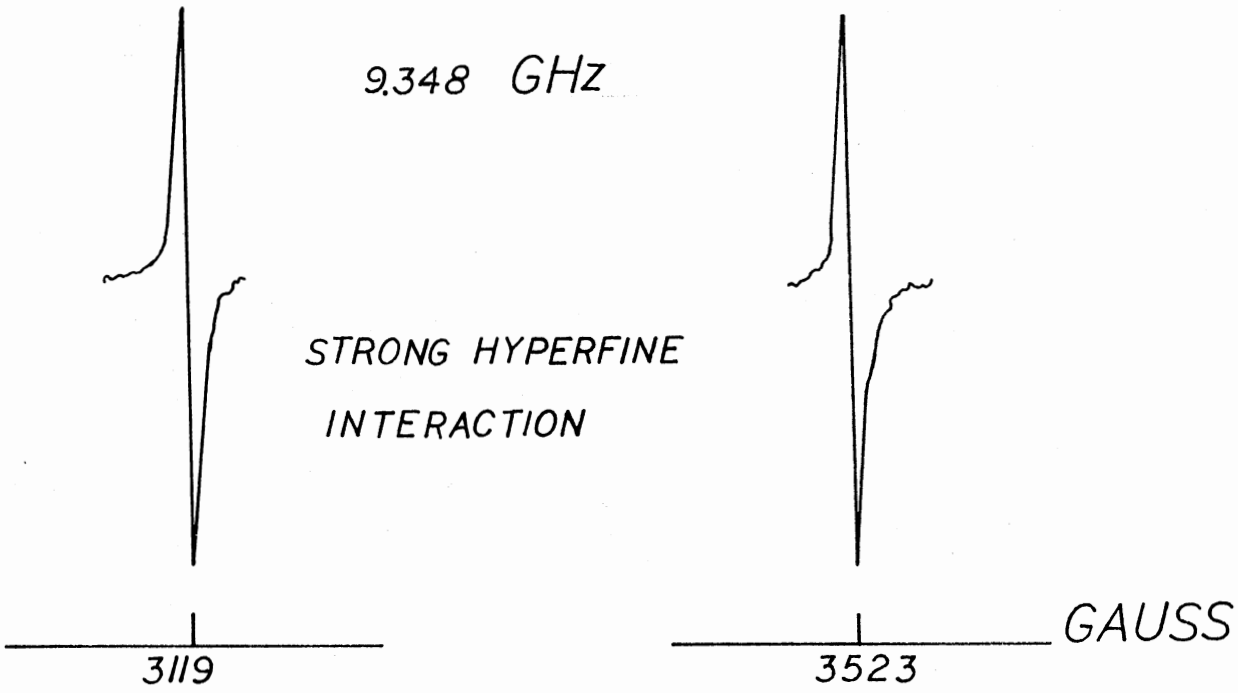

Figure 6. Strong Hyperfine Interaction Lines

correspond to the strong hyperfine lines.

The sample was rotated in ten degree intervals. Data were taken up to sixty degrees in the positive direction and up to fifty degrees in the negative direction of the [001]. The data taken are listed in Table II. The angular dependence for the ^{29}Si hyperfine interaction for both the high and low fields are given in Figures 7 and 8.

A computer program written in BASIC language was used to analyze the data. The program calculates the final set of the twelve parameters; the parameters being the three components of the $\overleftrightarrow{g}$ and $\overleftrightarrow{A}$ matrices and the orientation angles associated with each.

Only the strong hyperfine data were used in the final analysis of the $\overleftrightarrow{g}$ and $\overleftrightarrow{A}$ matrices. For each orientation of the magnetic field, there are two transitions according to the spin selection rules $\Delta M_s = \pm 1$ and $\Delta M_I = 0$ (see Figure 4). For each observed strong hyperfine line, the microwave frequency and the magnetic field (listed in Table II) are used as input data for the computer program that determines the twelve parameters.

The spin Hamiltonian for the strong hyperfine case is discussed in Chapter III and the corresponding 4x4 matrix is derived there. Computer diagonalization of the 4x4 matrix gives the energy levels. For a given magnetic field, one can thus calculate the energy for a transition. In our case, the energies are expressed in terms of a frequency ($\nu = E/h$) and can be directly compared to the microwave frequency for a transition.

To determine the twelve parameter values, we begin by "guessing" an initial set. Then for each observed ESR line listed in Table II, we calculated the microwave frequency corresponding to the measured magnetic field value and the assumed parameter values. This gives us a calculated

TABLE II

EXPERIMENTAL DATA

Angle Deg.	Frequency MHz	Magnetic Field Gauss
-50	9362.336	3102.68
	9362.337	3127.19
	9362.339	3128.61
	9362.341	3521.88
	9362.341	3521.88
	9362.341	3523.91
	9362.343	3547.58
-40	9354.630	3105.53
	9354.625	3127.55
	9354.625	3128.83
	9354.620	3522.13
	9354.621	3522.79
	9354.621	3542.13
-30	9347.118	3109.42
	9347.118	3126.35
	9347.119	3129.16
	9347.108	3521.60
	9347.109	3523.86
	9347.110	3540.79
-20	9342.162	3114.05
	9342.163	3125.20
	9342.164	3218.29
	9342.171	3522.47
	9342.172	3525.17
	9342.174	3536.31
-10	9338.331	3118.80
	9338.332	3112.45
	9338.333	3126.16
	9338.317	3524.32
	9338.320	3526.23
	9338.322	3531.51
0	9336.583	3123.22
	9336.594	3527.22
10	9335.737	3119.56
	9335.737	3122.55
	9335.736	3126.55
	9335.735	3523.76
	9335.736	3527.82
	9335.735	3530.59

TABLE II (Continued)

Angle Deg.	Frequency MHz	Magnetic Field Gauss
20	9336.841	3115.76
	9336.841	3122.37
	9336.841	3128.46
	9336.841	3521.85
	9336.840	3528.07
	9336.840	3534.30
30	9339.712	3112.61
	9339.712	3122.66
	9339.712	3128.54
	9339.714	3521.85
	9339.712	3527.95
	9339.712	3537.50
40	9344.268	3110.15
	9344.268	3123.33
	9344.267	3126.86
	9344.268	3523.57
	9344.269	3527.42
	9344.268	3540.02
50	9352.086	3108.69
	9352.084	3123.75
	9352.085	3124.24
	9352.080	3526.54
	9352.081	3541.47
60	9359.425	3108.38
	9359.425	3119.47
	9359.425	3125.44
	9359.430	3525.35
	9359.429	3530.83
	9359.430	3541.91

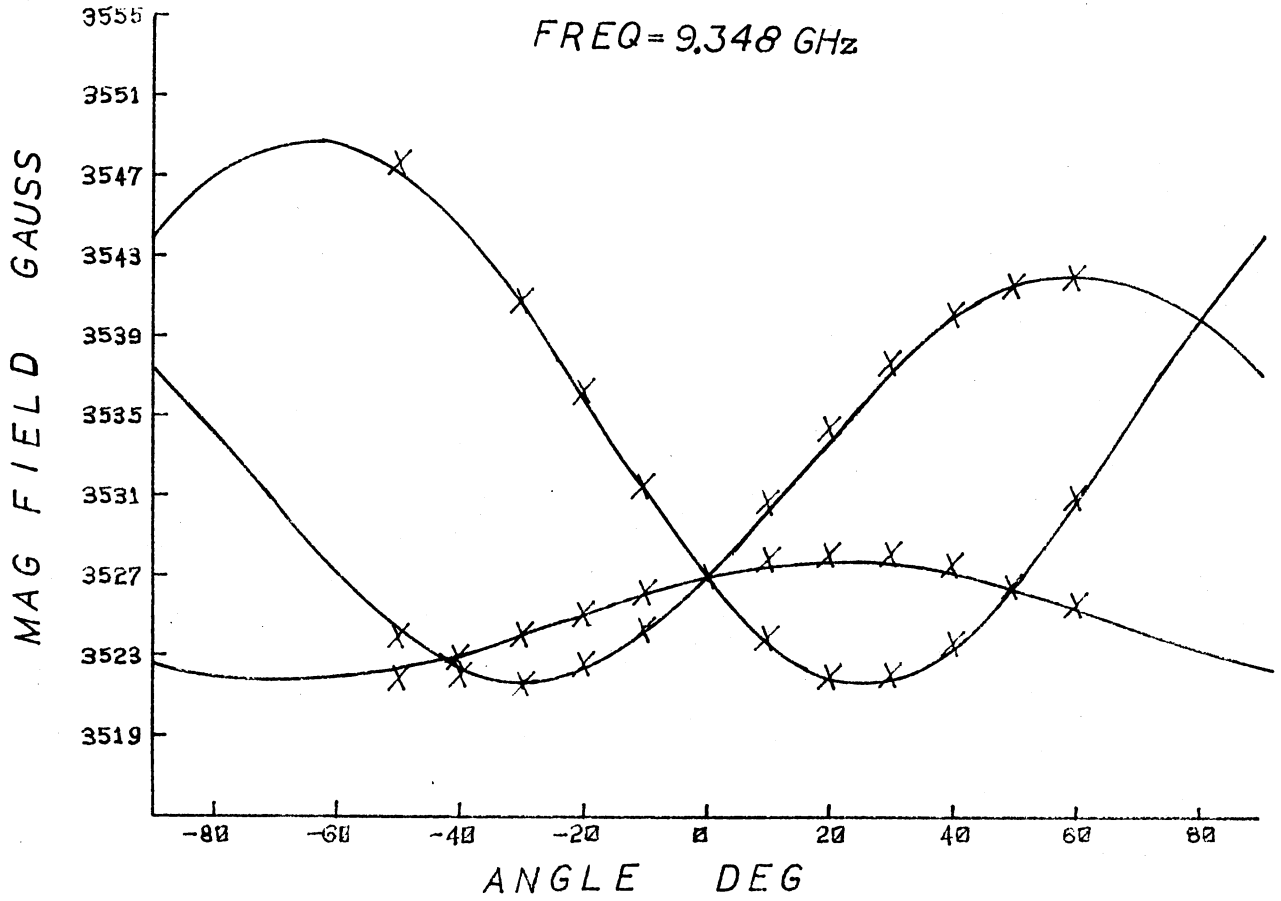

Figure 7. Angular Dependence for Low Field ^{29}Si Hyperfine Interaction

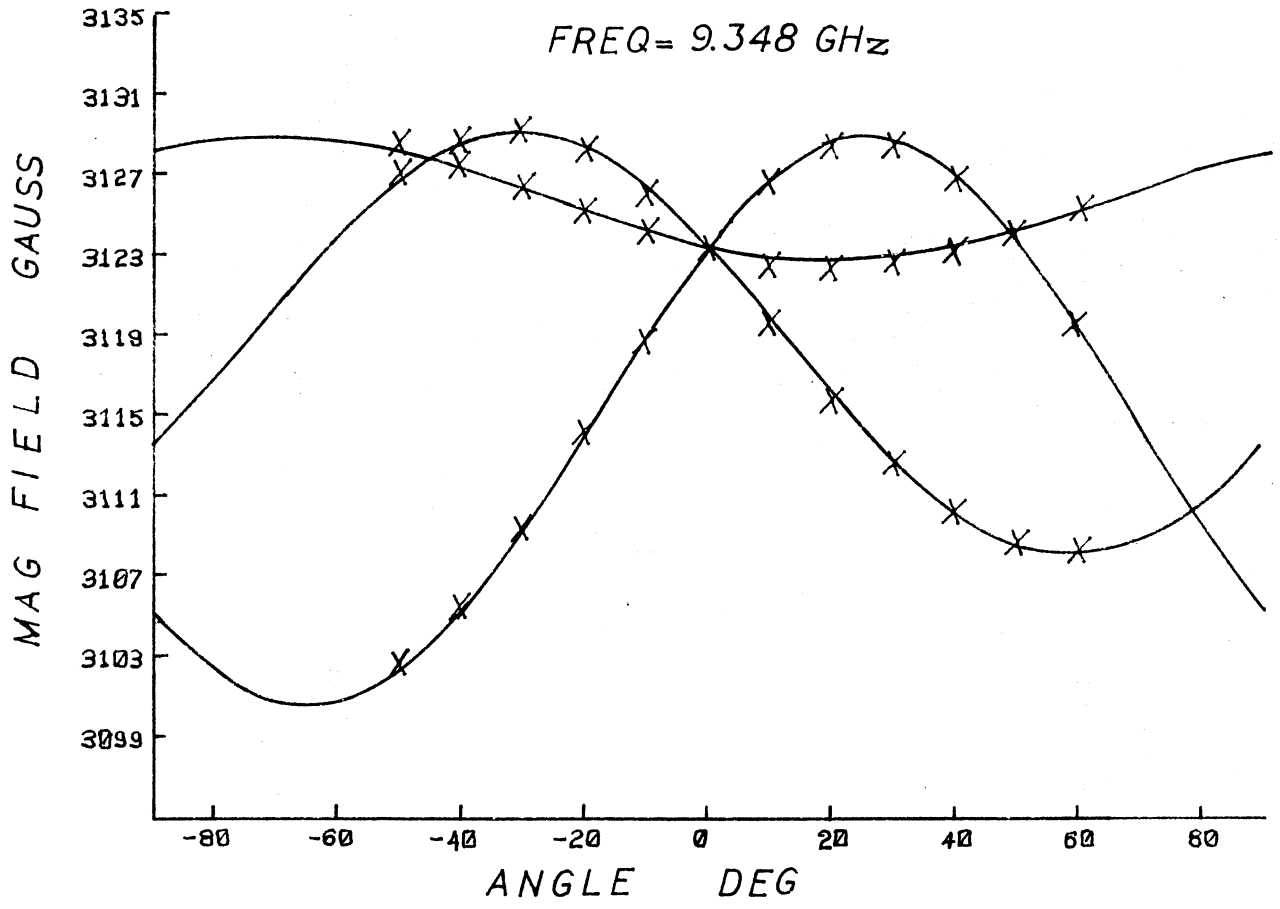

Figure 8. Angular Dependence for High Field ^{29}Si Hyperfine Interaction

frequency for each measured ESR line which we then can compare to the experimental microwave frequency for each line. For the best set of parameters, these calculated and experimental microwave frequencies will be the same. Of course our initial guess for the parameters is not the best so we define a quantity called SUM as follows:

$$SUM = \sum_{i=1}^{N} \left[\nu_{i(expt)} - \nu_{i(calc)} \right]^2$$

where N equals the number of experimentally measured ESR lines. The best set of parameters corresponds to the minimization of this SUM quantity. The minimization process is done systematically by varying each of the twelve parameters, one by one, by predetermined amounts. After each change of a parameter, a new set of calculated microwave frequencies are obtained and a new SUM is determined.

The final set of parameters is reached when any change in the parameters does not produce a lower value of the SUM. The parameters obtained from the computer program are shown in Table III. A comparison with the principal values of Silsbee (1961) is also included.

Because of uncertainties concerning the coordinate system and the direction of the +X axis used by Silsbee, we do not try to make comparisons with the principal axis directions.

TABLE III

SPIN HAMILTONIAN PARAMETERS FOR THE E_1' CENTER

Matrix	Principal Values (Silsbee, 1961)	Principal Values (Present Study)	Principal Directions (Present Study)	
			θ	ϕ
$\overleftrightarrow{g}$	2.00029	2.00032	55.1°	299.3°
	2.00049	2.00055	134.4°	346.2°
	2.00176	2.00178	64.7°	48.6°
$\overleftrightarrow{A}_{strong}$	1091.24 MHz	1093.45 MHz	55.6°	301.9°
	1091.24 MHz	1095.05 MHz	135.8°	347.1°
	1271.12 MHz	1269.75 MHz	65.9°	49.7°

TABLE IV

A COMPARISON OF BOND DIRECTIONS IN THE PERFECT QUARTZ LATTICE WITH THE UNIQUE PRINCIPAL AXIS DIRECTIONS FOR THE g AND STRONG HYPERFINE MATRICES OF THE E_1' CENTER

	Direction	
	θ	ϕ
$A_{Z,strong}$	65.9°	49.7°
g_Z	64.7°	48.6°
Si(6) - Ox(5)	66.4	50.7°

CHAPTER V

SUMMARY

In the present study, we have experimentally investigated the ground state ESR spectrum of the E_1' center in α-quartz. Data were taken as a function of angle. The resulting experimental microwave frequencies and magnetic field positions were used as input for a computer program to determine the spin Hamiltonian parameters. As part of this program, the spin Hamiltonian was expressed in a form suitable for computation. The parameters that resulted from this computer fit to the experimental data are listed in Table III.

The remaining task is to relate these parameters to the quartz lattice. In Table IV a comparison of the bond direction Si(6) - Ox(5) is made with the unique principal axes of the spin Hamiltonian matrices. The notation Si(6) and Ox(5) is taken from Figure 2. The agreement between the principal axis directions and this particular bond direction is excellent. Thus, we believe the E_1' center is an oxygen vacancy center (the oxygen vacancy being Ox(5) in Figure 2) and the electron is localized in the sp^3 hybrid orbital extending from Si(6) toward the vacancy. This means the unpaired electron is in a short bond and the model illustrated in Figure 2 is correct.

SELECTED BIBLIOGRAPHY

Megaw, H. D. "Crystal Structures: A Working Approach", W. B. Saunders Company, Philadelphia, 1973.

Cady, W. G. "Piezoelectricity", Dover Publications, New York, 1964.

Feigl, F. J., W. B. Fowler, and K. L. Yip. Solid State Communications 14, 225 (1974).

Weeks, R. A. Paramagnetic Resonance of Lattice Defects in Irradiated Quartz. J. Appl. Phys. 27, 11 (1956).

Silsbee, Robert H. Electron Spin Resonance in Neutron-Irradiated Quartz. J. Appl. Phys. 32, 8 (1961).

Yip, Kwok Leung and W. Beall Fowler. Electronic Structure of E_1' Centers in SiO_2. Phys. Rev. B 11, 6 (1975).

Castle, Jr., J. G., D. W. Feldman, and P. G. Klemens, and R. A. Weeks. Electron Spin-Lattice Relaxation at Defect Sites; E' Centers in Synthetic Quartz at 3 Kilo-Oersteds. Phys. Rev. 130, 2 (1963).

Weeks, R. A. and C. M. Nelson. Trapped Electrons in Irradiated Quartz and Silica: II, Electron Spin Resonance. J. Amer. Cer. Soc. 43, 8 (1960).

Halliburton, L. E., B. D. Perlson, R. A. Weeks, J. A. Weil and M. C. Wintersgill. EPR Study of the E_4' Center in α-Quartz. Solid State Commun. 30, pp. 575-579, Pergamon Press, Ltd. 1979. Printed in Great Britain.

VITA 2

Evangelos Theodore Skoumbourdis

Candidate for the Degree of

Master of Science

Thesis: ELECTRON SPIN RESONANCE OF THE E_1' CENTER IN α-QUARTZ

Major Field: Physics

Biographical:

Personal Data: Born in Nazareth Israel, April 4, 1945, the son of Dr. and Lady T. C. Skoumbourdis.

Education: Received Bachelor of Science degree in Mathematics from Tennessee Technological University, June, 1970; received Bachelor of Science degree in Physics from Tennessee Technological University, August, 1972; received Master of Science degree in Mathematics from Tennessee Technological University, August, 1974; completed requirements for Master of Science degree at Oklahoma State University, December, 1982.